

RESEARCH ARTICLE

10.1002/2014JC010363

Changes in the mesoscale variability and in extreme sea levels over two decades as observed by satellite altimetry

Philip L. Woodworth¹ and Melisa Menéndez²¹National Oceanography Centre, Liverpool, UK, ²Environmental Hydraulics Institute "IH Cantabria," Universidad de Cantabria, Santander, Spain

Key Points:

- Mesoscale variability does not change over two decades
- Trends in positive and negative extreme levels are determined by MSL trend
- Trends in sea level slope variability have been slightly positive on average

Supporting Information:

- Readme
- Figure S1a
- Figure S1b
- Figure S2
- Figure S3
- Figure S4ab
- Figure S4cd

Correspondence to:

P. L. Woodworth,
plw@noc.ac.uk

Citation:

Woodworth, P. L., and M. Menéndez (2015), Changes in the mesoscale variability and in extreme sea levels over two decades as observed by satellite altimetry, *J. Geophys. Res. Oceans*, 120, 64–77, doi:10.1002/2014JC010363.

Received 6 AUG 2014

Accepted 13 DEC 2014

Accepted article online 18 DEC 2014

Published online 13 JAN 2015

Abstract A data set of precise radar altimeter sea surface heights obtained from the same 10 day repeat ground track has been analyzed to determine the magnitude of change in the ocean "mesoscale" variability over two decades. Trends in the standard deviation of sea surface height variability each year are found to be small (typically ~ 0.5 percent/yr) throughout the global ocean. Trends in positive and negative extreme sea level in each region are in general found to be similar to those of mean sea level, with some small regional exceptions. Generalized Extreme Value Distribution (GEVD) analysis also demonstrates that spatial variations in the statistics of extreme positive sea levels are determined largely by the corresponding spatial variations in mean sea level changes, and are related to regional modes of the climate system such as the El Niño–Southern Oscillation. Trends in the standard deviation of along-track sea level gradient variability are found to be close to zero on a global basis, with regional exceptions. Altogether our findings suggest an ocean mesoscale variability that displays little change when considered over an extended period of two decades, but that is superimposed on a spatially and temporally varying signal of mean sea level change.

1. Introduction

Sea level exhibits a wide spectrum of variability that changes considerably throughout the ocean [Harrison, 2002; Hughes and Williams, 2010; Pugh and Woodworth, 2014], and the extremes of that variability are of particular interest for both scientific and practical reasons. At the coast, tide gauges provide the information on extreme sea levels required to design effective flood defences. Such extremes occur primarily due to storm surges, with the character of surges (amplitude, duration, spatial scale) differing between the tropics and higher latitudes [von Storch and Woth, 2008]. A major topic of research concerns whether the frequency and magnitude of these observed extreme sea level events are changing at a different rate than expected from changes in mean sea level [e.g., Menéndez and Woodworth, 2010]. By contrast, in the deep ocean, where satellite altimetry is the main source of sea level information, one is presented with different types of variability associated primarily with fluctuations in the ocean circulation.

This paper discusses one component of deep ocean sea level variability, that which occurs on time scales less than a year, resulting from the energetic "mesoscale" variations due to eddies, Rossby waves and instabilities in ocean currents, and from the seasonal cycle in sea level. In fact, one of the first achievements of altimetry was to identify the mesoscale variability [Cheney *et al.*, 1983; Menard, 1983] and it has been studied in detail since then [e.g., Le Traon and Morrow, 2001; Fu *et al.*, 2010; Morrow and Le Traon, 2012]. However, to our knowledge, there have been few studies of changes in the global mesoscale climatology over the two decades of precise altimetry, or of whether mesoscale-related extreme sea levels have changed throughout the world ocean differently to the much-discussed changes in mean sea level.

2. The Altimeter Data Set and Analysis Methods

We use the combined "reference series" data set of satellite altimetry from the TOPEX/Poseidon, Jason-1 and Ocean Surface Topography Mission/Jason-2 missions spanning two decades 1993–2012 [Beckley *et al.*, 2010]. This data set is available as one file (Merged_TOPEX_Jason_OSTM_Version_V2.8) from the Physical Oceanography Distributed Active Archive Center (PODAAC, podaac.jpl.nasa.gov). These measured sea surface height (SSH) data have had all instrumental and environmental corrections applied, including those for the tides and the inverse barometer and dynamic atmospheric correction, and with calibrations for height

offsets between and during missions. The SSHs have been interpolated by the data providers to provide time series at over 600,000 georeferenced points separated by 5.8 km (1 s) around the 10 day repeat ground track. The heights are expressed as anomalies relative to the Technical University of Denmark (DTU) DTU10 mean sea surface (MSS) which is a development of the MSS described by *Andersen and Knudsen* [2009] (Note that the MSS itself does not enter into the analyses described below, being merely a reference level by means of which the reported anomalies represent SSHs.) *Beckley et al.* [2013] provide details on the processing of the altimeter data set.

One second values were rejected if they failed certain quality flags in the data set, including that for bad root mean square between the individual height returns (obtained at 10 Hz for TOPEX/Poseidon and 20 Hz for the Jason-1 and –2 missions) within a 1 s SSH average. In addition, flags were used to reject SSH values if one or more of the correction terms were outside their nominal range, if the cross-track distance between the ground-track for a particular pass and the average ground-track was too large (i.e., > 1 km), if sea ice was detected in the returns, or if the radiometer observations were suspect [*Beckley et al.*, 2013].

For the figures shown in sections 3 and 4.1, relating to changes in the mesoscale climatology and to changes in maximum and minimum SSH, quantities were computed at each point along-track, with values smoothed and interpolated using the *grdfilter* function of the Generic Mapping Tools [*Wessel and Smith*, 1998] with a cosine arch filter of 300 km width.

For the analysis of extreme positive sea levels in section 4.2, a different mapping approach was followed as it was necessary to aggregate the individual measurements at each georeferenced point into grid boxes, selected optimally in the present case as 2° longitude by 1.5° latitude. The use of such grids, containing all available measurements inside each box, is a standard practice in the analysis of extreme wave heights using altimeter data [e.g., *Alves and Young*, 2003; *Izaguirre et al.*, 2011], since it provides an effective approach to overcoming the problem of a coarse spatial and time resolution. The resulting global grid contains 16,380 boxes, each with a number of SSH values equivalent to approximately two values per day, albeit with a small number of boxes in the tropics having few data.

3. Changes in the Mesoscale Climatology

The mesoscale has small spatial scales (typically a few 100 km), and spatial features of the mesoscale at any one time are studied best using data from a combination of several simultaneously operating satellites, if they are available [e.g., *Pascual et al.*, 2006]. However, the data sets of the reference series of missions can be used to investigate any changes in the magnitude of such variability over two decades, in spite of (or, in fact, because of) the relatively coarse spatial sampling provided by the 10 day repeat orbit.

The version of the familiar map shown in Figure 1 was derived by computing the standard deviation of SSH variability about the mean sea level at each point, with the mean and standard deviation calculated for each individual calendar year. We denote the standard deviation as $STD(i)$ for year “i.” Points were selected only if they had an adequate amount of information, with at least 15 years of data required, each with at least 27 out of a maximum of 37 values of SSH obtained from 10 day sampling in the year. Figure 1 shows the average of the annual $STD(i)$ values (denoted $\langle STD \rangle$). Therefore, the figure represents the average high-passed variability over a year, rather than lower-frequency processes such as the El Niño-Southern Oscillation (ENSO) or secular sea level change. This variability includes the seasonal cycle, which can have large spatial scale, as well as the mesoscale associated with eddies and the instabilities of currents. However, as the latter is the far more energetic at many locations, we refer below to all the variability presented by this filtering as “mesoscale.”

The map of $\langle STD \rangle$ in Figure 1 shows the high variability associated with the Gulf Stream and Loop Current in the North Atlantic, the Brazil-Malvinas Confluence in the South Atlantic, the Agulhas Current retroflexion, the Antarctic Circumpolar Current, the Kuroshio in the North Pacific and East Australian Current in the South Pacific, the various Equatorial Currents, and many other features of the ocean circulation.

However, STD can vary considerably between years due to, for example, the fluctuating populations of eddies in the ocean, or differences in the seasonal cycle from year to year. Figure 2 shows the “percentage STD range,” defined as the difference between the maximum and minimum $STD(i)$ divided by the $\langle STD \rangle$ of Figure 1, and expressed as a percentage. It indicates that the STD varies by ~50–150% across the whole

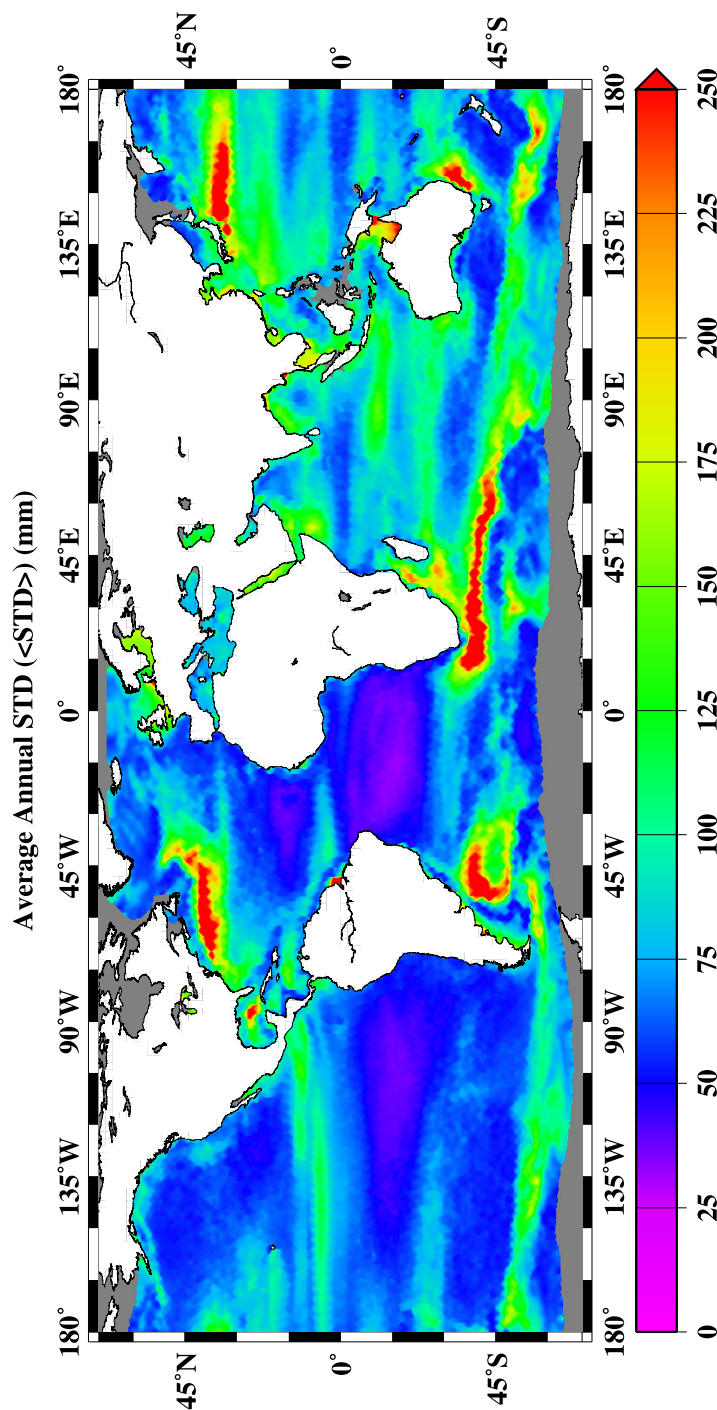


Figure 1. The average standard deviation of SSH variability (<STD>) computed in each year between 1993 and 2012.

ocean with largest values in equatorial areas. Moreover, while the Aleutian Current, for example, stands out as having an STD that varies from year to year more than elsewhere, most of the map is fairly uniform, with the strong signals due to the Gulf Stream and the other major current systems mentioned above largely absent.

The interannual variation in STD will have many causes but the most obvious is that due to ENSO. Figure 3 shows the correlation between the 20 annual values of STD and the Niño-3 index (obtained from the Earth System Research Laboratory, www.esrl.noaa.gov), demonstrating high positive values in an equatorial band stretching across the Indian and Pacific Oceans. This shows that, while sea level itself depends on ENSO, correlated positively in the eastern equatorial Pacific and negatively in the western Pacific warm pool as is well known [e.g., McPhaden *et al.*, 1998], interannual changes in sea level variability within a year (i.e., between the STD(i) values) also depends on ENSO. A similar plot is obtained for correlation with the Indian Ocean Dipole (IOD) index in the equatorial Pacific, less so for the tropical Indian and Atlantic Oceans, due to the annual Niño-3 and IOD indices having some similarity during 1993–2012 (correlation coefficient 0.32).

With such a large range of variation in STD as shown by Figure 2, any increase/decrease in the variability in SSH, as represented by the trends in STD over two decades (Figure 4a), will be estimated only with large uncertainties. Most of the ocean has trends that are small and consistent with zero at the 95% confidence level (significance was computed with allowance for serial correlation using the method of Maul and Martin [1993]). Those areas with trends that are significantly different from zero are indicated by the superimposed ground tracks in black. Areas with significant trends include extensive parts of the central and northern Atlantic and southern Indian Ocean and bands associated with the major currents. Figure 4b shows the same trends expressed as

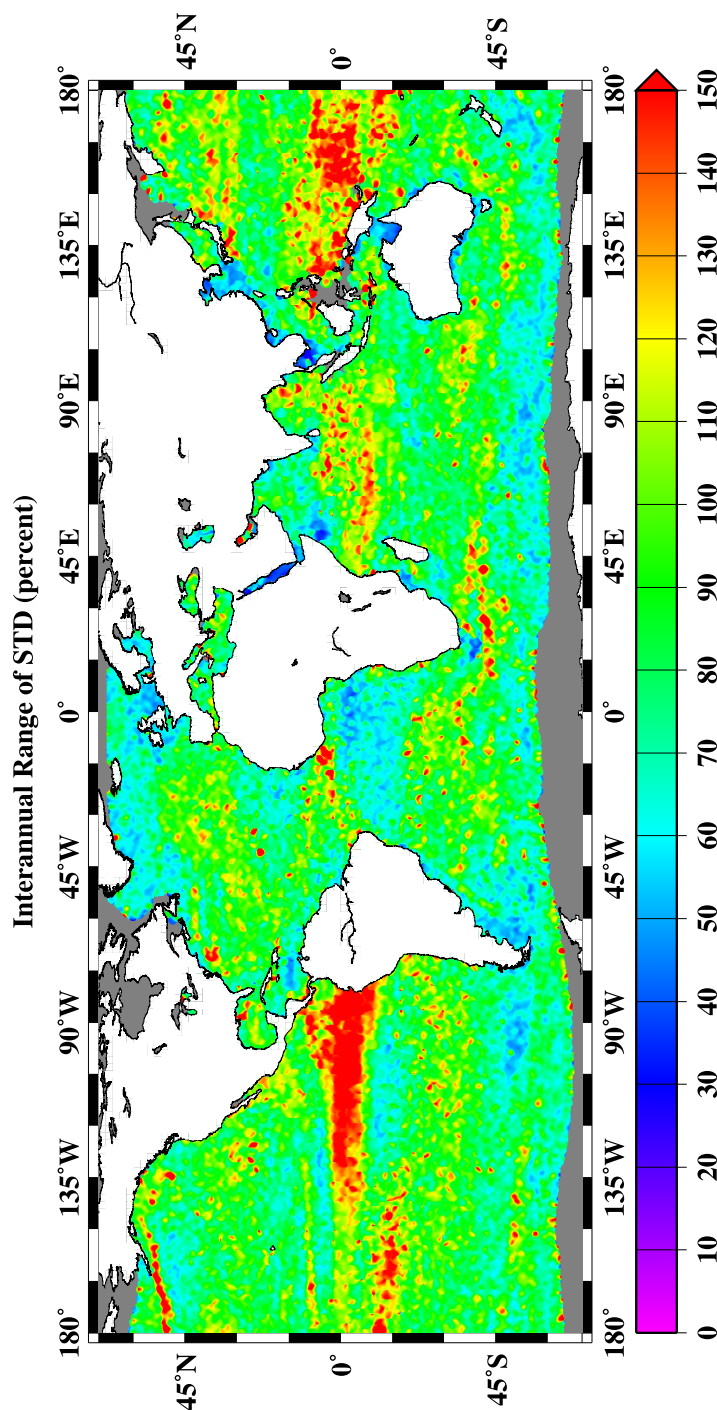


Figure 2. Interannual variability of SSH at each point, showing the range (maximum minus minimum) of the standard deviations of SSH (i.e., the STD(*i*) in each year “*i*”) during 1993–2012 and expressed as a percentage of $\langle \text{STD} \rangle$.

2 standard errors from zero; as expected, this map looks very like Figure 4a. One concludes that sampling trends in annual STD at individual reference points in this way, and then interpolating and smoothing with *grdfilter* provides a robust representation of the spatial pattern of trends.

Some features in Figure 4a or 4b can be related to the paths of individual eddies which vary in frequency and amplitude from year to year (see also Figure 2). For example, a narrow positive band corresponding to the track of Agulhas eddies from South Africa to almost the Brazil coast can be seen. These are known to be

a percentage of $\langle \text{STD} \rangle$. This indicates that the changes are typically ~ 0.5 percent/yr of $\langle \text{STD} \rangle$ with a few areas at the 1 percent/yr level or more. Altogether, the figures demonstrate that the high-frequency mesoscale “noise” in the ocean sampled in this way, that combines with low-frequency variability and long-term sea level change to provide the overall ocean variability, is largely stable.

One can make a similar map to Figure 4a, making use only of trends at individual reference points when they are greater than 2 standard errors from zero. If the individual trends that go into the interpolated and smoothed map made by *grdfilter* have a normal (or at least symmetric) distribution about a (positive or negative) mean value in a particular area, then one would expect that the resulting map would have exaggerated (positive or negative) values but with otherwise a similar spatial distribution to Figure 4a. This is indeed the case, for example generally positive values in the tropical Atlantic and negative ones in the western tropical Pacific are obtained. The map has no entries for the eastern equatorial Pacific, and parts of the equatorial Atlantic and Indian Oceans, where measured trends are consistently smaller than twice the estimated standard errors. Similarly, one can make a map using only trends at individual reference points when they are less than

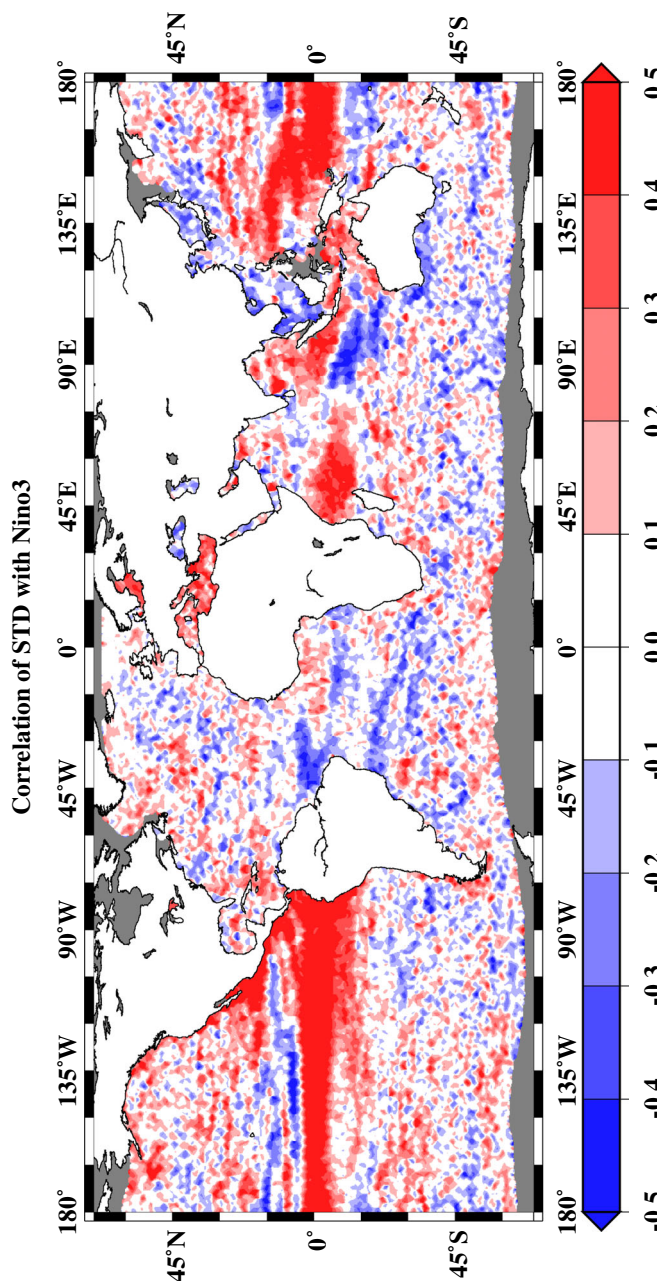


Figure 3. Interannual correlation between SSH variability and ENSO, showing the Pearson correlation between standard deviations of SSH (i.e., the STD(i) in each year "i") and Niño-3 index values during 1993–2012.

consider the most extreme variations. Figure 5a shows the estimated trends in annual mean sea level computed from the average of the SSH values in each year at each reference point (a maximum of 37 values per year). This figure has been presented many times in the literature, with the spatial variations in mean sea level trends known to be similar to those of thermosteric sea level change [e.g., *Meysignac and Cazenave, 2012*]. Supporting information Figures S1a and S1b show the corresponding maps for the maximum and minimum SSHs each year, respectively. Even though these two figures are based on much smaller statistics than Figure 5a (i.e., one SSH measurement each year rather than a maximum of 37), the patterns of their trends are largely the same.

However, there are small regional differences between these maps. Figures 5b and 5c show the trends of maximum and minimum SSH values when they are expressed with respect to the mean value each year.

primarily anticyclonic (positive sea level) eddies that follow the South Atlantic “eddy corridor” [*Gordon and Haxby, 1990; Byrne et al., 1995; Souza et al., 2011*]. The preference for eddies with long lifetimes and propagation differences in this region to be anticyclonic has been described by *Chelton et al. [2011]* who, in a comprehensive study of eddies in the global ocean, also identified the general preference for anticyclonic eddies to travel towards the equator and cyclonic eddies to the poles. Their study demonstrated many further aspects of eddies, such as the reduced number to be found along the cores of the major currents, with eddies preferring to locate in bands of meanders either side of central current paths, as can also be inferred from Figures 4a and 4b. The Oregon State University eddies data base (<http://cioss.coas.oregonstate.edu/eddies/>) contains information on the tracks and amplitudes of individual cyclonic and anticyclonic eddies observed by altimetry.

4. Variability in Extreme Sea Levels

4.1. Maximum and Minimum Sea Surface Heights

So far we have considered a measure of the entire variability in a year (the STD(i) values).

However, it is also of interest to

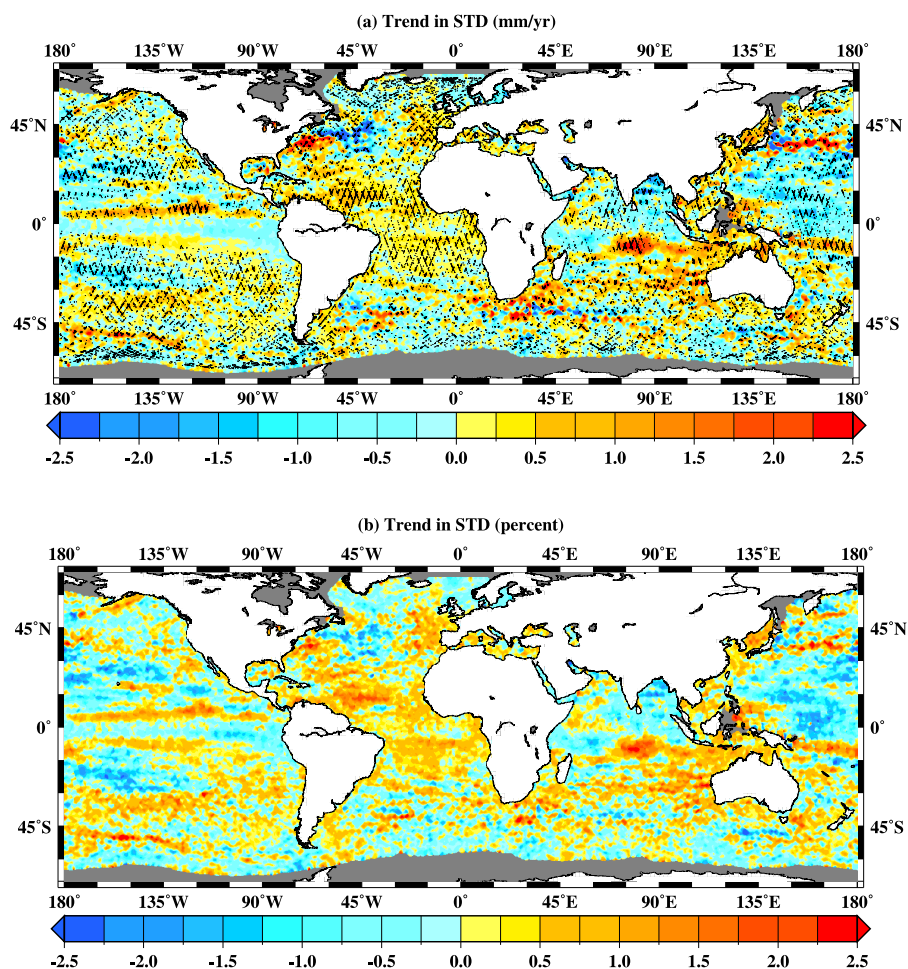


Figure 4. (a) Secular trends in values of STD over the period 1993–2012. Areas with superimposed ground tracks in black have trends significantly different from zero at the 95% confidence level. (b) Trends expressed as a percentage of the average annual STD (i.e., $\langle \text{STD} \rangle$) at each point.

They demonstrate primarily a symmetry about the mean values, with positive values in Figure 5b corresponding largely to negative values in Figure 5c, and vice versa. One exception is in Figure 5b, which shows an even clearer narrow band in the South Atlantic corresponding to the anticyclonic Agulhas eddies, with no corresponding negative band in Figure 5c.

Supporting information Figure S2 plots the differences between the values in Figures 5b and 5c, providing trends in the range of maximum–minimum SSH each year. As may have been anticipated, this figure has similarities to the trends in STD in Figure 4a, apart from an overall scaling factor of ~ 4 (as would be inferred assuming a normal distribution containing 37 values). In particular, larger positive trends are observed in the Atlantic and southern Indian Oceans.

In general, one would have expected Figure 4a and supporting information Figure S2 to be the same (apart from the scaling factor) if the populations of SSH values with respect to the mean values at each point had been normally distributed throughout. The fact that the trends in the range of maximum–minimum extreme SSH values are little different to what might have been expected from the STD of the entire set of (maximum 37) SSH values each year implies a climatology that is largely stable, with variability in extreme positive and negative SSHs tending to take place on average in line with changes in mean values.

4.2. GEVD Analysis of Extreme Positive Sea Levels

Analysis of positive extreme sea levels using a Generalized Extreme Value Distribution (GEVD) formulation provides a link between the variability discussed above for the open ocean, and the extreme high sea levels

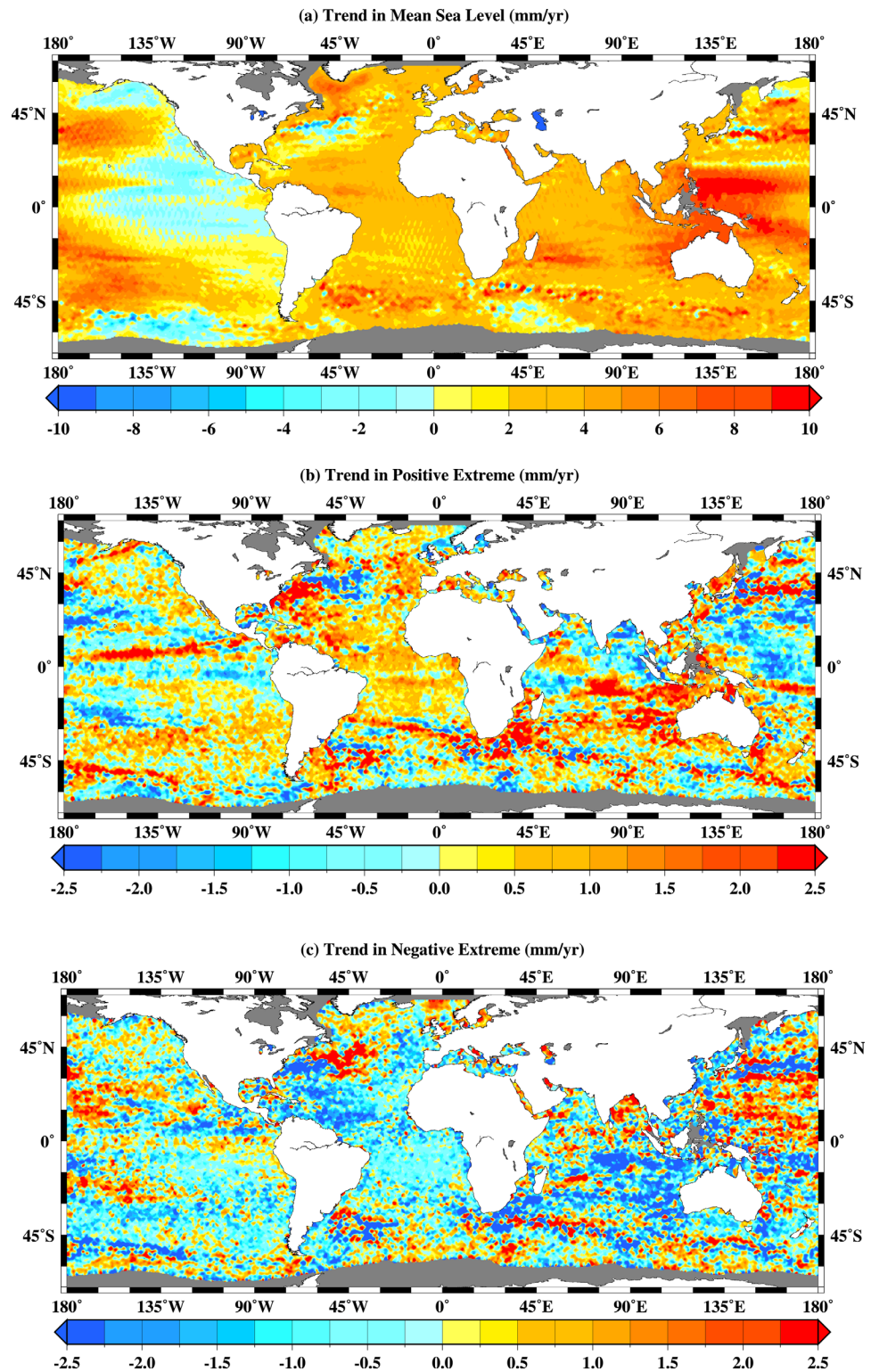


Figure 5. Secular trends in (a) mean sea level measured each year over the period 1993–2012, (b) the extreme positive SSH for each year measured with respect to the mean for the year, and (c) the extreme negative SSH for each year measured with respect to the mean for the year.

that are studied in coastal tide gauge data [Menéndez and Woodworth, 2010]. Using again data for the two decades 1993–2012, we gridded the SSH values by the method described in section 2. Boxes of 2° longitude by 1.5° latitude were used, with each box containing a number of SSH values equivalent on average to

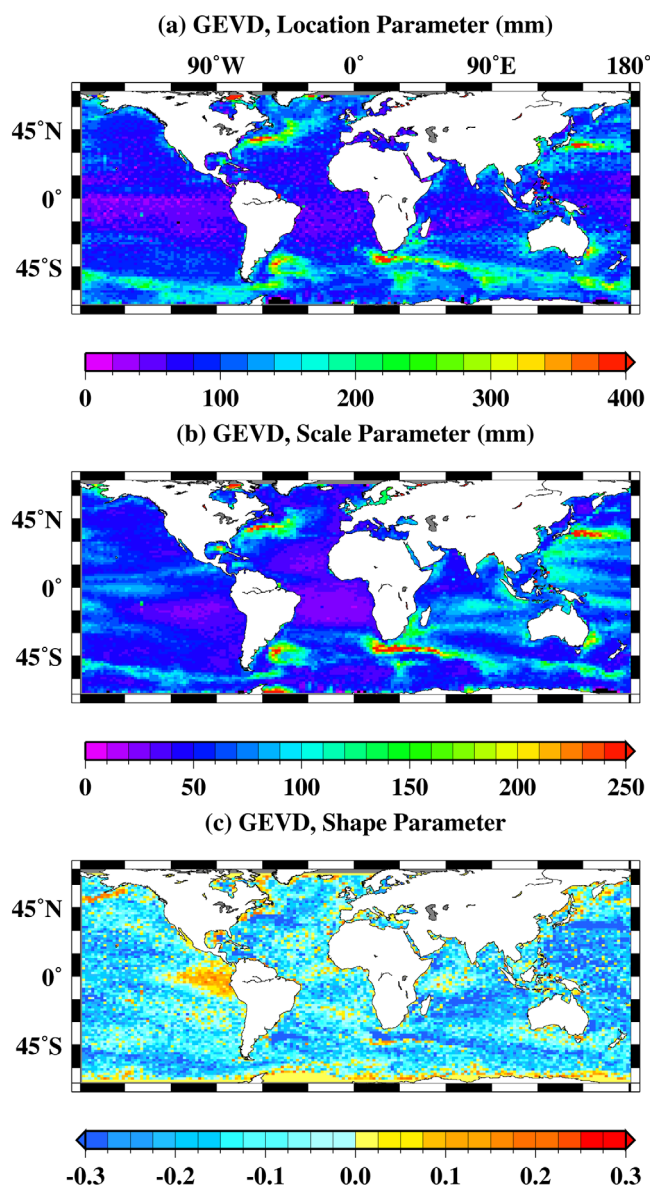


Figure 6. Distributions of (a) location, (b) scale and (c) shape parameters from the GEVD model using monthly maxima values.

the location and scale parameters are provided in supporting information Figure S3a and Figure S3b. The seasonal variations are higher in the equatorial regions for both parameters, while high seasonal variations in the location parameters are also found in the Gulf Stream and Kuroshio Current regions.

The shape parameter determines the upper tail of the distribution and describes the behavior of the most unusual extreme events (Figure 6c). Generally negative values are found worldwide, indicating a bounded upper tail in the GEVD. This can be a consequence of one of two reasons: either regularly occurring intense extreme events, or the nonoccurrence of unusual maxima. However, some regions present positive shape parameter values (i.e., occurrence of SSH anomalies of unusual magnitude). These include the eastern tropical Pacific, northern extratropical coastal areas in the western Pacific and Atlantic Oceans, a band across the Aleutian Islands, and at the highest latitudes sampled (seasonal variations in the shape parameter are not modeled).

Figure 7 shows the estimated linear trends in the location parameter of the time-dependent GEVD model which may be compared to the trends in MSL of Figure 5a. The two sets of trends are largely the same. The statistical significance of the trends shown by the stippled areas in Figure 7 indicates that, except for a

approximately two values per day. We have verified from analysis of data in these boxes that this mapping provides similar spatial information with regard to variations in the mesoscale climatology in section 3. The main characteristics of spatial variation in extreme positive SSH across the grid are obtained by fitting block maxima values of SSH in each box to the GEVD. In this case, we have used monthly maxima values and a time-dependent GEVD model taking into account seasonal variations and following the nonstationary statistical model described by Méndez *et al.* [2007].

Maps of the estimated GEVD parameters are shown in Figure 6. The location parameter (Figure 6a), which informs about the average intensity of extreme values, has similarities to the average annual STD ($\langle \text{STD} \rangle$ in Figure 1), with higher values associated with same ocean areas noted above. The scale parameter (Figure 6b) characterizes the spread of the GEVD, and thereby informs about the variability of extremes. It presents a similar spatial pattern to the location parameter but relatively higher values in the tropical Indian and western tropical Pacific Oceans. Seasonal variations in

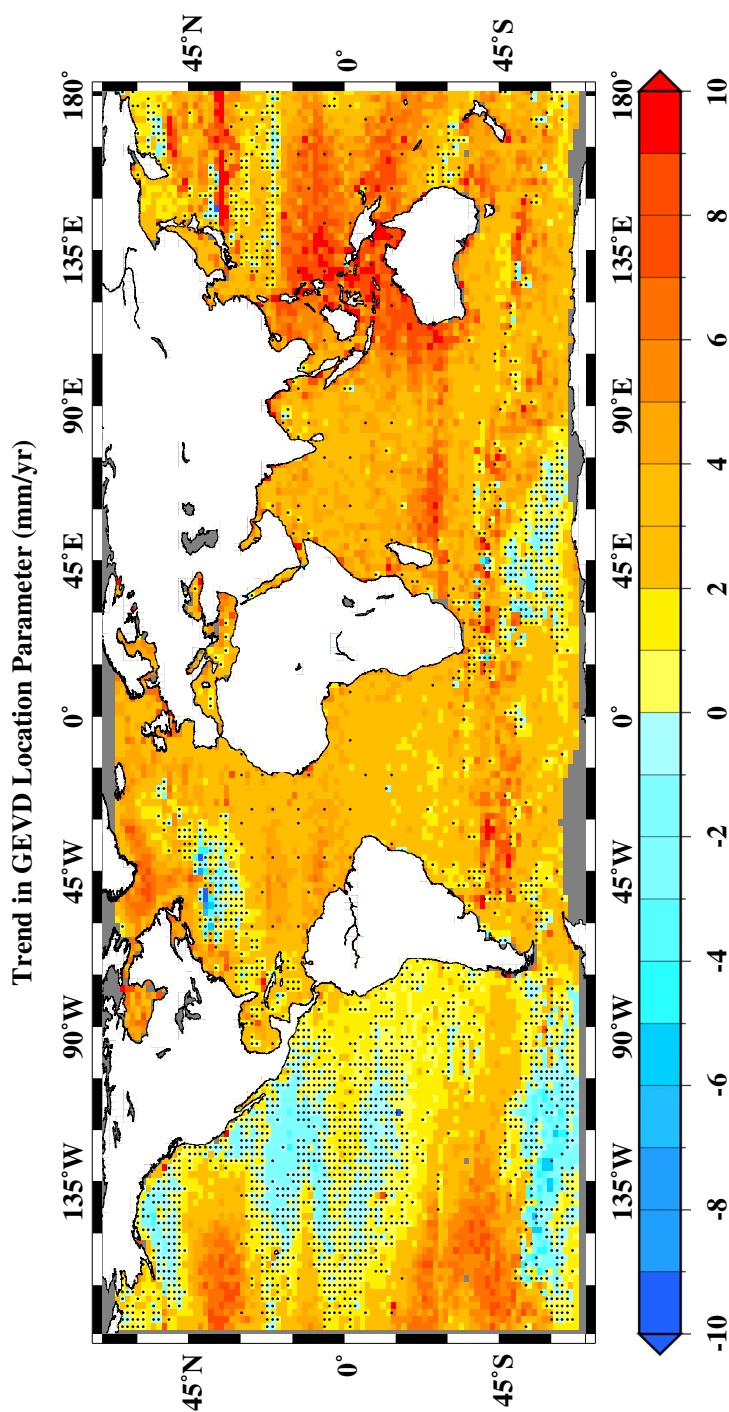


Figure 7. Secular trends in the location parameter from the GEVD model. Hatching indicates regions where the trend is not significantly different from zero at the 95% confidence interval.

anticipated strong positive relationship in the eastern tropical Pacific, along the whole American Pacific coast, in the western Indian Ocean and at high latitudes in the South Pacific. On the other hand, a negative relationship is found in the western Pacific warm pool and in the eastern Indian Ocean. The SAM index as covariate (supporting information Figure S4d) provides a positive relationship in the Roaring Forties area of the Indian Ocean sector of the Southern Ocean, and a negative relationship in the south and central-equatorial Pacific Ocean.

region in the higher-latitude south Pacific, most of the negative regional trends are not significantly different from zero, confirming a general global increase in extreme positive SSH anomalies in line with changes in mean values.

In order to study the interannual variability of extreme sea levels in more detail, a climate index can be introduced as a covariate in the location parameter of the GEVD, to investigate the relation between local maximum SSH values and teleconnections due to internal modes of variability of the climate system. We have assessed the influence of the Arctic Oscillation (AO), North Atlantic Oscillation (NAO), ENSO (represented by the Niño-3 index), and Southern Annular Mode (SAM) on extreme SSHs by adding each individual monthly climate index as a covariate (see supporting information for the sources of the indices). Supporting information Figure S4a shows the relationship between extreme SSHs and AO is similar to, and generally stronger than, that for the NAO (supporting information Figure S4b). A positive relationship is found in Northern Europe (North and Baltic Seas), the central North Atlantic and western tropical Pacific, while a negative relationship is found in the Mediterranean Sea and eastern tropical North Atlantic. The relationship between ENSO and extreme sea level is shown in supporting information Figure S4c, revealing an

5. Changes in Along-Track Sea Level Gradients

The mesoscale is often studied in terms of eddy kinetic energy (EKE) instead of SSH [e.g., Heywood *et al.*, 1994; Luo *et al.*, 2011]. EKE is computed from the squares of the anomalies of sea level gradient at each point along the altimeter ground track [Menard, 1983; Shum *et al.*, 1990]. EKE varies seasonally and from year to year, particularly in equatorial regions [Ducret *et al.*, 2000; Fu *et al.*, 2010; Morrow and Le Traon, 2012]. In parts of the ocean, it can be related to the intensity of the wind forcing responsible for the variability in ocean currents [Meredith and Hogg, 2006].

For the present study, we have chosen to investigate whether there have been changes in STD of along-track height difference, rather than in EKE, which as a squared quantity presents values that have a larger spread and are less suitable for fitting by least squares. Along-track height difference was calculated as the difference in SSH between a reference point and another point N seconds further along the track. Findings for $N = 10$

are shown here following Strub *et al.* [1997], similar findings are obtained for $N = 15$. (For along-track gradient studies we found it necessary to lower the requirement of at least 27 out of a maximum of 37 pairs of sea level differences to 20.)

Figure 8a shows the trend in STD for along-track sea level differences for 1993–2012 using $N = 10$. Although signals of the ocean circulation can be seen in this figure related to the Gulf Stream, Kuroshio and Antarctic Circumpolar Current, most of the trends in the map are small and positive, with the average trend in the figure being 0.23 mm/yr. The shorter period 1993–2003 provides a similar map (Figure 8b), but with trends that have positive and negative values in extended areas such as west and east of Australia and south of South Africa. These areas coincide with those where Stammer *et al.* [2006] found positive and negative values of eddy mixing parameter using data over the same 11 years (their Figure 2b), this parameter being proportional to EKE multiplied by a timescale defined by the ambient environmental shear and stratification [Stammer, 1998]. Note that Figure 8b has more smoothing than Figure 8a for greater consistency with Figure 2b of Stammer *et al.* [2006].

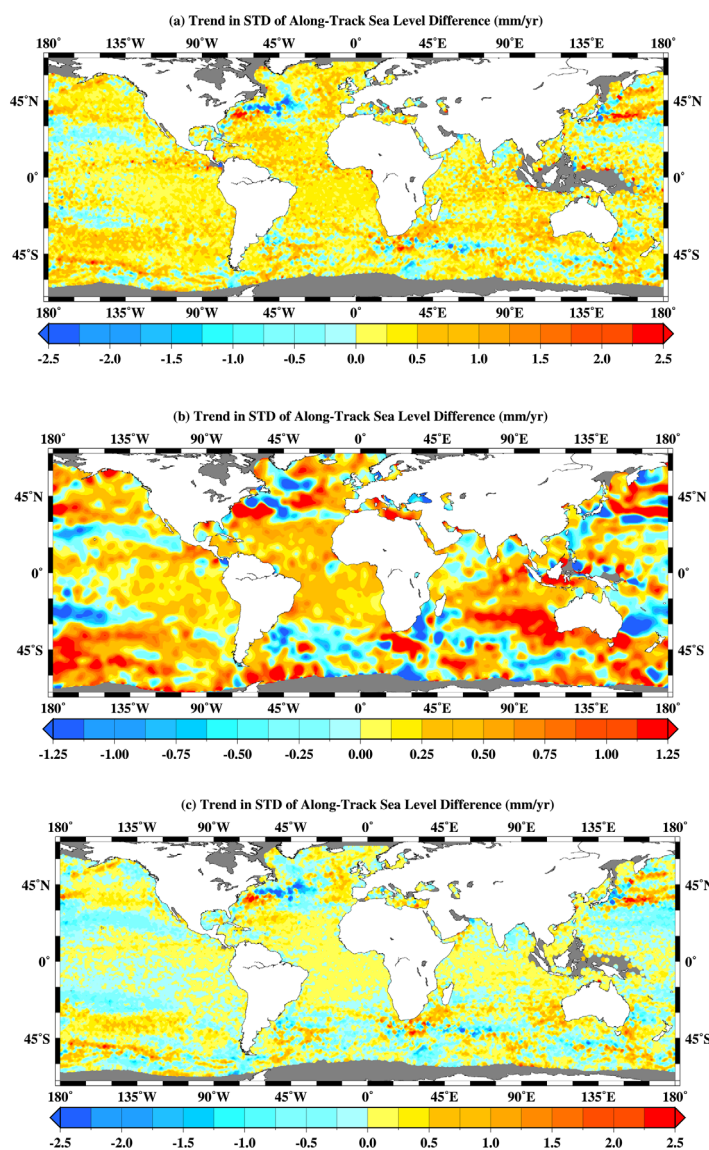


Figure 8. (a) Trends in the STD of along-track sea level difference for 1993–2012 where differences are measured between reference points 10 s apart ($N = 10$) and with smoothing using a 300 km width cosine arch filter. (b) Trends in STD of along-track sea level difference for 1993–2003 and $N = 10$ with smoothing by a 1000 km filter for greater consistency with Figure 2b of Stammer *et al.* [2006]. (c) As Figure 8a but with sea level anomalies smoothed with the use of a 7 s along-track triangular filter.

Consequently, the trends in STD in Figures 8a and 8b are not a new observation. Their mostly positive values suggest the (rather unlikely) possibility, that ocean currents have become generally more variable over the last two decades, at least on the spatial scale sampled. One can inspect the STD time series at individual locations where the trend has been found to be positive, but this has not proved more informative, simply verifying that STD values in these areas were larger during the Jason-1 and Jason-2 eras (launched 2001 and 2008, respectively) than in the earlier TOPEX/Poseidon period.

A possible explanation for the generally positive values is that the altimeter data themselves, rather than the ocean, have become noisier. Differences in the data quality between missions in the reference series have always been investigated in great detail. For example, see *Zanifé et al.* [2003] for comparisons between TOPEX/Poseidon and Jason-1, or *Ablain et al.* [2010] between Jason-1 and -2. The accuracy and stability of the sea state bias correction in each mission has been of particular interest [e.g., *Chambers et al.*, 2003], as has the consistency between orbit computations [*Lemoine et al.*, 2010]. Most of the quality assessment of altimeter data to be found in the literature has focused, quite rightly, on the stability of measurements between missions for application to the study of long-term mean sea level change [e.g., *Leuliette et al.*, 2004; *Beckley et al.*, 2013], rather than the measurement noise of interest here.

Since the first altimeter data sets, it has been known that the several cm instrumental noise results in a “correlation length scale” in the measurements within which the along-track 1 s SSH values are correlated [*Fu*, 1983; *Dibarboue et al.*, 2014], and that this length-scale of typically 70–100 km is comparable to that of the mesoscale in many parts of the ocean [*Le Traon et al.*, 1990, 2008]. *Zanifé et al.* [2003] concluded that the instrumental noise was similar for TOPEX/Poseidon and Jason-1 when the radar waveforms were analyzed in the same way. However, in practice, Jason-1 data have been found to be noisier than those of TOPEX/Poseidon for wavelengths less than 50 km, owing to the different ways in which data were processed in each mission [*Dorandeu et al.*, 2004; *Ponte et al.*, 2007].

A different type of noise, relevant to the georeferenced data set that we are using, stems from its reliance on a cross-track gradient correction owing to the repeat ground track deviating slightly from its average position in each particular pass. There were extended periods during the Jason-1 mission when the cross-track distance between the actual and nominal ground-tracks exceeded 1 km, and numerous manoeuvres were required (B. Beckley, private communication, 2014). However, in the present analysis, the appropriate quality flag was selected to ensure cross-track distance less than 1 km, so this aspect is not expected to be important.

Therefore, it is plausible that the 1 s data values (derived from the compression of higher rate SSHs at 10 and 20 Hz for TOPEX/Poseidon and Jason-1 and -2 respectively), as provided to users via the PODAAC georeferenced data set, have become slightly noisier over the two decades. We found that much of the positive bias in Figure 8a can be removed by along-track filtering. We used a simple 7 s triangular filter with weights 1234321, resulting in a map with an average trend of only 0.01 mm/yr, although with a similar spatial pattern (i.e., generally more positive values in the tropical and subtropical Atlantic and to the west of Australia) (Figure 8c). Consequently, we conclude that, consideration of noise aside, any true changes in ocean current variability must have been small. Figure 8c itself is consistent with the only other relevant studies known to us. *Biri* [2013, her Figure 4.9] shows trends in EKE for the period 1993–2010, with positive and negative spatial patterns very similar to Figure 8c, and with a positive global-average trend in EKE of 0.10 percent/yr. *O'Donnell et al.* [2012] also reported largely negative trends in EKE over an 18 year period in the northern and southern subtropical Pacific, and positive trends in the NE Atlantic, the South Indian Ocean off Western Australia, Scotia Sea, and Pacific-Antarctic Ridge regions of the Southern Ocean.

6. Conclusions

The picture presented is of sea level variability on time scales less than a year (that we have called the “meso-scale” variability), with a standard deviation (STD) that can vary from year to year by ~100 percent or more. This variability can thereby be an important parameter in determining how different ocean and atmospheric forcings result in ocean circulation variability [*Volkov*, 2005; *Thompson and Demirov*, 2006; *Morrow and Le Traon*, 2012; *Hristova et al.*, 2014]. On interannual timescales, variability in STD can be associated with climate modes such as ENSO. However, over an extended period such as two decades, STD values show little change

(typically ~ 0.5 percent/yr with a few areas, clearly associated with ocean dynamical variability, at the 1 percent/yr level or more). The trends in annual maximum and minimum SSHs have been shown to be generally similar to those of annual mean sea level. Furthermore, the extremes of positive SSH have changed at most locations in a similar way to mean sea level at that location. Our findings are reminiscent of those at the coast, where studies of tide gauge data have shown that long-term trends in extreme sea levels are determined to a great extent by changes in mean values [Woodworth *et al.*, 2011], and that higher water levels may be governed by the interannual fluctuations in ocean-atmosphere circulation patterns [Menéndez and Woodworth, 2010]. However, changes in the mesoscale variability will result from dynamical processes that are more complex than the wind-driven storm surges that apply at the coast. As a result, we believe that trends in the mesoscale of the sort described here could provide tests between different ocean climate models.

As for changes in the STD of along-track height difference, our finding in Figure 8a is consistent with that reported by Stammer *et al.* [2006] (and our Figure 8b) and, at face value at least, suggests a small trend toward greater ocean circulation variability. However, many of those positive trends can be reduced toward zero by along-track filtering, with the resulting map (Figure 8c) consistent with previously obtained spatial patterns of trends in EKE. As the global average of change in STD in this case is close to zero, this again suggests a stability of the mesoscale component of the circulation over timescales of several decades.

The mesoscale is only one component of the overall deep ocean sea level variability, which includes that due to large-scale, low-frequency variations such as ENSO [e.g., Zhang and Church, 2012], and long-term regional and global sea level change due to climate change [Stammer *et al.*, 2013; Church *et al.*, 2014]. The requirements for monitoring the many aspects of sea level variability have been recognized for several years [e.g., Wilson *et al.*, 2010], and fortunately look set to be further recognized over the next decade by a series of complementary altimeter missions [Benveniste, 2011]. It will be interesting to see how some of the trends reported in this paper change in the future.

Acknowledgments

The altimeter data used in this paper were obtained from PODAAC (podaac.jpl.nasa.gov) and we thank Brian Beckley from the Goddard Space Flight Center for advice on using them. This work was funded partly by the UK Natural Environment Research Council. Melisa Menéndez acknowledges the support of the Spanish Secretaría General de Ciencia, Tecnología e Innovación under the project iMar21 (CTM2010-15009).

References

- Ablain, M., S. Philipps, N. Picot, and E. Bronner (2010), Jason-2 global statistical assessment and cross-calibration with Jason-1, *Mar. Geod.*, 33(51), 162–185, doi:10.1080/01490419.2010.487805.
- Alves, J. H. G. M., and I. R. Young (2003), On estimating extreme wave heights using combined Geosat, Topex/Poseidon and ERS-1 altimeter data, *Appl. Ocean Res.*, 25(4), 167–186, doi:10.1016/j.apor.2004.01.002.
- Andersen, O. B., and P. Knudsen (2009), DNSCO8 mean sea surface and mean dynamic topography models, *J. Geophys. Res.*, 114, C11001, doi:10.1029/2008JC005179.
- Beckley, B. D., N. P. Zelensky, S. A. Holmes, F. G. Lemoine, R. D. Ray, G. T. Mitchum, S. Desai, and S. T. Brown (2010), Assessment of the Jason-2 extension to the TOPEX/Poseidon, Jason-1 sea-surface height time series for global mean sea level monitoring, *Mar. Geod.*, 33(51), 447–471, Supplemental Issue on OSTM/Jason-2 calibration/validation, doi:10.1080/01490419.2010.491029.
- Beckley, B. D. *et al.* (2013), Integrated multi-mission ocean altimeter data for climate research: TOPEX/Poseidon, in *Jason-1 and OSTM/Jason-2 User's Handbook, version 2*, 46 pp., Calif. Inst. of Tech., Pasadena, Calif. [Available at podaac.jpl.nasa.gov.]
- Benveniste, J. (2011), Radar altimetry: Past present and future, in *Coastal Altimetry*, edited by S. Vignudelli, *et al.*, pp. 1–17, Springer, Berlin.
- Biri, S. (2013), On dynamical causes of eddy variability in the ocean, dissertation, 124 pp., Doctor of Natural Sciences, University of Hamburg, Hamburg, Germany. [Available at <http://ediss.sub.uni-hamburg.de/volltexte/2013/6266/>.]
- Byrne, D. A., A. L. Gordon, and W. F. Haxby (1995), Agulhas eddies: A synoptic view using Geosat ERM data, *J. Phys. Oceanogr.*, 25, 902–917, doi:10.1175/1520-0485(1995)025<0902:AEASVU>2.0.CO;2.
- Chambers, D. P., S. A. Hayes, J. C. Ries, and T. J. Urban (2003), New TOPEX sea state bias models and their effect on global mean sea level, *J. Geophys. Res.*, 108(C10), 3305, doi:10.1029/2003JC001839.
- Chelton, D. B., M. G. Schlax, and R. M. Samelson (2011), Global observations of nonlinear mesoscale eddies, *Prog. Oceanogr.*, 91, 167–216, doi:10.1016/j.pocean.2011.01.002.
- Cheney, R. E., J. G. Marsh, and B. D. Beckley (1983), Global mesoscale variability from collinear tracks of SEASAT altimeter data, *J. Geophys. Res.*, 88(C7), 4343–4354, doi:10.1029/JC088iC07p04343.
- Church, J. A., *et al.* (2014), Sea level change, in *Climate Change 2013: The Physical Science Basis, Chap 13, Working Group I Report of the Fifth Scientific Assessment of the Intergovernmental Panel on Climate Change*, edited by T. F. Stocker, *et al.*, pp. 1137–1216, Cambridge Univ. Press, Cambridge, U. K.
- Dibarboure, G., F. Boy, J. D. Desjonqueres, S. Labroue, Y. Lasne, N. Picot, J. C. Poisson, and P. Thibaut (2014), Investigating short-wavelength correlated errors on low-resolution mode altimetry, *J. Atmos. Oceanic Technol.*, 31, 1337–1362, doi:10.1175/JTECH-D-13-00081.1.
- Dorandeu, J., M. Ablain, Y. Faugere, F. Mertz, B. Soussi, and P. Vincent (2004), Jason-1 global statistical evaluation and performance assessment: Calibration and cross-calibration results, *Mar. Geod.*, 27, 345–372, doi:10.1080/01490410490889094.
- Ducet, N., P. Y. Le Traon, and G. Reverdin (2000), Global high-resolution mapping of ocean circulation from TOPEX/Poseidon and ERS-1 and -2, *J. Geophys. Res.*, 105, 19477–19498, doi:10.1029/2000JC900063.
- Fu, L.-L. (1983), On the wave number spectrum of oceanic mesoscale variability observed by the SEASAT altimeter, *J. Geophys. Res.*, 88(C7), 4331–4341, doi:10.1029/JC088iC07p04331.
- Fu, L.-L., D. B. Chelton, P.-Y. Le Traon, and R. Morrow (2010), Eddy dynamics from satellite altimetry, *Oceanography*, 23, 14–25, doi:10.5670/oceanog.2010.02.

- Gordon, A. L., and W. F. Haxby (1990), Agulhas eddies invade the south Atlantic: Evidence from Geosat altimeter and shipboard conductivity-temperature-depth survey, *J. Geophys. Res.*, *95*(C3), 3117–3125, doi:10.1029/JC095iC03p03117.
- Harrison, C. G. A. (2002), Power spectrum of sea level change over fifteen decades of frequency, *Geochem. Geophys. Geosyst.*, *3*(8), 1–17, doi:10.1029/2002GC000300.
- Heywood, K., E. McDonagh, and M. White (1994), Eddy kinetic energy of the North Atlantic subpolar gyre from satellite altimetry, *J. Geophys. Res.*, *99*(C11), 22,525–22,539, doi:10.1029/94JC01740.
- Hristova, H. G., W. S. Kessler, J. C. McWilliams, and M. J. Molemaker (2014), Mesoscale variability and its seasonality in the Solomon and Coral Seas, *J. Geophys. Res. Oceans*, *119*, 4669–4687, doi:10.1002/2013JC009741.
- Hughes, C. W., and S. D. P. Williams (2010), The color of sea level: Importance of spatial variations in spectral shape for assessing the significance of trends, *J. Geophys. Res.*, *115*, C10048, doi:10.1029/2010JC006102.
- Izaguirre, C., F. J. Méndez, M. Menéndez, and I. J. Losada (2011), Global extreme wave height variability based on satellite data, *Geophys. Res. Lett.*, *38*, L10607, doi:10.1029/2011GL047302.
- Lemoine, F. G., et al. (2010), Towards development of a consistent orbit series for TOPEX, Jason-1, and Jason-2, *Adv. Space Res.*, *46*(12), 1513–1540, doi:10.1016/j.asr.2010.05.007.
- Le Traon, P. Y., and R. Morrow (2001), Ocean currents and eddies. in *Satellite Altimetry and Earth Sciences. A Handbook of Techniques and Applications*, edited by L.-L. Fu and A. Cazenave, pp. 171–215, Academic, San Diego, Calif.
- Le Traon, P. Y., M. C. Rouquet, and C. Boissier (1990), Spatial analysis of mesoscale variability in the North Atlantic as deduced from Geosat data, *J. Geophys. Res.*, *95*(C11), 20,267–20,285, doi:10.1029/JC095iC11p20267.
- Le Traon, P. Y., P. Klein, B. L. Hua, and G. Dibarboure (2008), Do altimeter wavenumber spectra agree with the interior or surface quasigeostrophic theory? *J. Phys. Oceanogr.*, *38*, 1137–1142, doi:10.1175/2007JPO3806.1.
- Leuliette, E. W., R. S. Nerem, and G. T. Mitchum (2004), Calibration of TOPEX/Poseidon and Jason altimeter data to construct a continuous record of mean sea level change, *Mar. Geod.*, *27*, 79–94, doi:10.1080/01490410490465193.
- Luo, H., A. Bracco, and E. Di Lorenzo (2011), The interannual variability of the surface eddy kinetic energy in the Labrador Sea, *Prog. Oceanogr.*, *91*, 295–311, doi:10.1016/j.pocean.2011.01.006.
- Maul, G. A., and D. M. Martin (1993), Sea level rise at Key West, Florida, 1846–1992: America's longest instrument record?, *Geophys. Res. Lett.*, *20*(18), 1955–1958, doi:10.1029/93GL02371.
- McPhaden, M. J., et al. (1998), The Tropical Ocean-Global Atmosphere observing system: A decade of progress, *J. Geophys. Res.*, *103*(C7), 14,169–14,240, doi:10.1029/97JC02906.
- Menard, Y. (1983), Observations of eddy fields in the Northwest Atlantic and Northwest Pacific by SEASAT altimeter data, *J. Geophys. Res.*, *88*(C3), 1853–1866, doi:10.1029/JC088iC03p01853.
- Méndez, F. J., M. Menéndez, A. Luceño, and I. J. Losada (2007), Analyzing monthly extreme sea levels with a time-dependent GEV model, *J. Atmos. Oceanic Technol.*, *24*, 894–911, doi:10.1175/JTECH2009.1.
- Menéndez, M., and P. L. Woodworth (2010), Changes in extreme high water levels based on a quasi-global tide-gauge dataset, *J. Geophys. Res.*, *115*, C10011, doi:10.1029/2009JC005997.
- Meredith, M. P., and A. M. Hogg (2006), Circumpolar response of Southern Ocean eddy activity to a change in the Southern Annular Mode, *Geophys. Res. Lett.*, *33*, L16608, doi:10.1029/2006GL026499.
- Meysignac, B., and A. Cazenave (2012), Sea level: A review of present-day and recent-past changes and variability, *J. Geodyn.*, *58*, 96–109, doi:10.1016/j.jog.2012.03.005.
- Morrow, R., and P.-Y. Le Traon (2012), Recent advances in observing mesoscale ocean dynamics with satellite altimetry, *Adv. Space Res.*, *50*, 1062–1076, doi:10.1016/j.asr.2011.09.033.
- O'Donnell, C., K. Heywood, D. Stevens, and E. Shuckburgh (2012), Global temporal trends in eddy kinetic energy from satellite altimetry, paper presented at the Symposium on 20 Years of Progress in Radar Altimetry, European Space Agency, Venice, 24–26 Sept 2012. [Available at www.altimetry2012.org.]
- Pascual, A., Y. Faugère, G. Larnicol, and P.-Y. Le Traon (2006), Improved description of the ocean mesoscale variability by combining four satellite altimeters, *Geophys. Res. Lett.*, *33*, L02611, doi:10.1029/2005GL024633.
- Ponte, R. M., C. Wunsch, and D. Stammer (2007), Spatial mapping of time-variable errors in Jason-1 and TOPEX/Poseidon sea surface height measurements, *J. Atmos. Oceanic Technol.*, *24*, 1078–1085, doi:10.1175/JTECH2029.1.
- Pugh, D. T. and P. L. Woodworth (2014), *Sea-Level Science: Understanding Tides, Surges, Tsunamis and Mean Sea-Level Changes*, Cambridge Univ. Press, Cambridge.
- Shum, C. K., R. A. Werner, D. T. Sandwell, B. H. Zhang, R. S. Nerem, and B. D. Tapley (1990), Variations of global mesoscale eddy energy observed from Geosat, *J. Geophys. Res.*, *95*(C10), 17,865–17,876, doi:10.1029/JC095iC10p17865.
- Souza, J. M. A. C., C. de Boyer Montégut, and P.-Y. Le Traon (2011), Comparison between three implementations of automatic identification algorithms for the quantification and characterization of mesoscale eddies in the South Atlantic Ocean, *Ocean Sci.*, *7*, 317–334, doi:10.5194/os-7-317-2011.
- Stammer, D. (1998), On eddy characteristics, eddy transports, and mean flow properties, *J. Phys. Oceanogr.*, *28*, 727–739, doi:10.1175/1520-0485(1998)028<0727:OECETA>2.0.CO;2.
- Stammer, D., C. Wunsch, and K. Ueyoshi (2006), Temporal changes in ocean eddy transports, *J. Phys. Oceanogr.*, *36*, 543–550, doi:10.1175/JPO2858.1.
- Stammer, D., A. Cazenave, R. M. Ponte, and M. E. Tamisiea (2013), Causes for contemporary regional sea level changes, *Annu. Rev. Mar. Sci.*, *5*, 21–46, doi:10.1146/annurev-marine-121211-172406.
- Strub, P. T., T. K. Chereskin, P. P. Niiler, C. James, and M. D. Levine (1997), Altimeter-derived variability of surface velocities in the California Current System: 1. Evaluation of TOPEX altimeter velocity resolution, *J. Geophys. Res.*, *102*(C6), 12,727–12,748, doi:10.1029/97JC00448.
- Thompson, K. R., and E. Demirov (2006), Skewness of sea level variability of the world's oceans, *J. Geophys. Res.*, *111*, C05005, doi:10.1029/2004JC002839.
- Volkov, D. L. (2005), Interannual variability of the altimetry-derived eddy field and surface circulation in the extratropical North Atlantic Ocean in 1993–2001, *J. Phys. Oceanogr.*, *35*, 405–426, doi:10.1175/JPO2683.1.
- von Storch, H., and K. Woith (2008), Storm surges: Perspectives and options, *Sustain. Sci.*, *3*, 33–43, doi:10.1007/s11625-008-0044-2.
- Wessel, P., and W. H. F. Smith (1998), New, improved version of Generic Mapping Tools released, *EOS Trans. AGU*, *79*, 579.
- Wilson, W. S., et al. (2010), Observing systems needed to address sea-level rise and variability. in *Understanding Sea-Level Rise and Variability*, Chap 12, edited by J. A. Church et al., Wiley-Blackwell, London, U. K.

- Woodworth, P. L., M. Menéndez, and W. R. Gehrels (2011), Evidence for century-timescale acceleration in mean sea levels and for recent changes in extreme sea levels, *Surv. Geophys.*, 32(4-5), 603–618 (erratum page 619), doi:10.1007/s10712-011-9112-8.
- Zanifé, O. Z., P. Vincent, L. Amarouche, J. P. Dumont, P. Thibaut, and S. Labroue (2003), Comparison of the Ku-Band range noise level and the relative sea-state bias of the Jason-1, TOPEX, and Poseidon-1 radar altimeters, *Mar. Geod.*, 26, 201–238, doi:10.1080/01490410390255737.
- Zhang, X., and J. A. Church (2012), Sea level trends, interannual and decadal variability in the Pacific Ocean, *Geophys. Res. Lett.*, 39, L21701, doi:10.1029/2012GL053240.